olivopontocerebellar atrophy and Shy-Drager syndrome). *J Neurol Sci* 1989; **94**:79–100.
20. Tu PH, Galvin JE, Baba M, Giasson B, Tomita T, Leight S, *et al.* Glial cytoplasmic inclusions in white matter oligodendrocytes of multiple system atrophy brains contain insoluble alpha-synuclein. *Ann Neurol* 1998; **44**:415–422.
21. Wakabayashi K, Yoshimoto M, Tsuji S, Takahashi H. Alpha-synuclein immunoreactivity in glial cytoplasmic inclusions in multiple system atrophy. *Neurosci Lett* 1998; **249**:180–182.
22. Snow BJ, Tooyama I, McGeer EG, Yamada T, Calne DB, Takahashi H, *et al.* Human positron emission tomographic [^{18}F]fluorodopa studies correlate with dopamine cell counts and levels. *Ann Neurol* 1993; **34**:324–330.
23. Rajput AH, Rozdilsky B, Rajput A, Ang L. Levodopa efficacy and pathological basis of Parkinson syndrome. *Clin Neuropharmacol* 1990; **13**:553–558.
24. Churchyard A, Donnan GA, Hughes A, Howells DW, Woodhouse D, Wong JY, *et al.* Dopa resistance in multiple-system atrophy: loss of postsynaptic D_2 receptors. *Ann Neurol* 1993; **34**:219–226.

Original Research Article

Dementia
and Geriatric
Cognitive Disorders

Dement Geriatr Cogn Disord 2008;26:547–555
DOI: 10.1159/000180280

Accepted: September 18, 2008
Published online: December 10, 2008

Differentiation of Early-Stage Alzheimer's Disease from Other Types of Dementia Using Brain Perfusion Single Photon Emission Computed Tomography with Easy Z-Score Imaging System Analysis

M. Waragai[a] S. Mizumura[b] T. Yamada[c] H. Matsuda[d]

[a]Division of Neurology, JR Tokyo General Hospital, and [b]Department of Radiology, Nippon Medical School, Tokyo, [c]Department of Neurology, School of Medicine, Fukuoka University, Fukuoka, and [d]Department of Nuclear Medicine, Saitama Medical University International Medical Center, Saitama, Japan

Key Words
SPECT · Easy Z-score imaging system · Dementia

Abstract
Introduction: We performed brain perfusion single photon emission computed tomography (SPECT) to evaluate computer-assisted automated discrimination of early Alzheimer's disease (AD) from other types of dementia using the easy Z-score imaging system (eZIS). ***Subjects and Methods:*** eZIS analysis of brain perfusion SPECT images was used in patients with early AD, vascular dementia (VD), mixed dementia (VD + AD), frontotemporal dementia (FTD), dementia with Lewy bodies (DLB), and normal controls. Significant changes in regional cerebral blood flow (rCBF) in the volume of interest were assessed in the posterior cingulate gyrus, precuneus and parietal cortices; the severity and extent of decreases in rCBF and the ratio of the extent of the decrease in rCBF to the decrease in whole-brain blood flow (rCBF ratio) were determined. ***Results:*** The severity of the decrease in rCBF in AD patients was significantly greater than in VD and FTD patients and controls. The extent of the decrease in rCBF in AD patients was significantly greater than in FTD patients and controls. The rCBF ratio in AD patients was higher than in VD and FTD patients and controls. ***Conclusion:*** The eZIS indices, especially the rCBF ratio, may be useful in establishing the differential diagnosis between early-stage AD and FTD or VD, but the differentiation of AD from VD + AD or DLB remains difficult.

Introduction

Considerable progress in diagnostic accuracy has been made using positron emission tomography (PET) and single-photon emission computed tomography (SPECT) in the diagnosis of Alzheimer's disease (AD). Computer-assisted analysis using voxel-based morphometry (VBM) [1] from statistical parametric mapping (SPM) [2] for magnetic resonance imaging (MRI) and three-dimensional stereotactic surface projection (3D-SSP) [3–5] or the easy Z-score imaging system (eZIS) [6–12] for PET/SPECT has been developed. Therefore, increasingly objective and reliable information on abnormalities in regional cerebral blood flow (rCBF) can be obtained. In Japan, ^{18}F-fluorodeoxyglucose positron emission tomography (^{18}F-FDG PET) for the diagnosis of dementia is not reimbursed yet by the health insurance system, and thus the more widely available brain perfusion SPECT and

KARGER
Fax +41 61 306 12 34
E-Mail karger@karger.ch
www.karger.com

1420–8008/08/0266–0547$24.50/0

Accessible online at:
www.karger.com/dem

Masaaki Waragai
Department of Geriatrics and Gerontology, Division of Brain Sciences
Institute of Development, Aging and Cancer, Tohoku University
4-1 Seiryo-cho Aobaku
Sendai 980-8575 (Japan)
Tel. +81 22 717 7182, Fax +81 22 717 8198, E-Mail waragai@kk.iij4u.or.jp

Table 1. Demographic and clinical data of subjects

	AD	VD + AD	DLB	VD	FTD	Normal
Number of subjects	45	22	21	21	21	24
Age range, years	61–85	64–89	70–79	74–86	57–85	60–80
Mean age ± SD, years	73.8 ± 2.7	80.5 ± 3.5	73.8 ± 8.5	79.1 ± 3.5	73 ± 8.5	71.1 ± 6.9
Male/female	22/23	13/9	15/6	13/8	13/8	14/10
Disease duration range, months	6–36	12–36	12–36	10–36	11–36	
Mean disease duration, months	15.0	25.8	16.1	19.5	18.6	
MMSE score, range	18–24	16–22	16–26	14–27	17–27	27–30
Mean MMSE score ± SD	21.0 ± 4.2	20.0 ± 4.8	21.8 ± 6.0	22.0 ± 5.7	21.2 ± 5.9	28.2 ± 2.2

MRI are primarily used for imaging diagnosis of AD. PET is more sensitive than SPECT in diagnosing early AD, but SPECT offers the advantages of lower cost and ease of access, which may lead to a large increase in the number of cases being studied with this technique.

A specific decrease in rCBF in the posterior cingulate gyrus, precuneus and parietal cortices in the very early stage of AD has been detected by SPECT [6–12]. eZIS is a method of statistical analysis for the automated diagnosis of brain perfusion SPECT images which can be used to investigate the rCBF objectively and easily [6–12]. SPECT combined with eZIS has been applied in clinical practice in multiple institutes, including general hospitals [8–12], as a valuable early diagnostic method in patients with AD. Waragai et al. [10] showed that eZIS analysis of SPECT images could be useful for the early and differential diagnosis of patients with neurodegenerative disease, including dementing diseases, AD, frontotemporal dementia (FTD), dementia with Lewy bodies (DLB). In patients with very early AD, rCBF decreased significantly in the posterior cingulate cortex and the precuneus gyrus whereas eZIS analysis in patients with DLB showed decreases in rCBF extending from the bilateral precuneus gyrus to the partial cortex, occipital cortex, primary visual cortex and the posterior cingulate cortex. These findings suggest neurodegenerative changes in DLB. The differential diagnosis between AD and DLB, in which decreased rCBF in the occipital lobe is not prominent at very early stages, is not easy because reduced rCBF in the posterior cingulate cortex has been observed in both DLB and AD at very early stages, as shown by our results. Therefore, we believe that brain perfusion SPECT using eZIS combined with ^{123}I-*m*-iodobenzylguanidine (MIBG) myocardial scintigraphy may be very useful for the differential diagnosis between early DLB and AD.

FTD is the third most common neurodegenerative dementia after AD and DLB. We demonstrated decreased rCBF in the frontal cortex, insula, temporal cortex and orbitofrontal cortex, regions which are related to antisocial behavioral symptoms with relative sparing of the posterior cortex in patients with FTD [10].

Matsuda et al. [8] have recently developed an automated system of analysis using eZIS with incorporation of a volume of interest (VOI) related to early AD, and showed its high performance in discriminating patients with very early AD from age-matched healthy volunteers.

The purpose of the current study was to evaluate this system as an adjunct for the early diagnosis of AD and other types of dementia such as vascular dementia (VD), AD + VD, DLB, and FTD.

Subjects and Methods

Subjects

Patients with clinical diagnoses of dementia and durations of illness of less than 3 years were included in this study, which was conducted with the approval of the JR Tokyo General Hospital Ethics Committee. SPECT using ^{99m}Tc-ethyl cysteinate dimer (^{99m}Tc-ECD) was performed within 3 years from onset of disease as part of the initial clinical evaluation of each subject after informed consent had been obtained. Disease onset was considered to be the time when symptoms first appeared.

The subjects were 45 patients with AD, 22 patients with VD + AD, 21 patients with DLB, 21 patients with VD and 21 patients with FTD. Twenty-four healthy volunteers without neurological disorders were enrolled as controls.

The patients' demographic characteristics are listed in table 1. Years of education of all subjects were more than 12 years.

The patients were followed by a board-certified neurologist for more than 3 years; the clinical diagnosis was established based on a detailed medical history, physiological and neurological examinations, the results of routine laboratory investigations, and serial MRIs of the brain. The final diagnosis was based on the par-

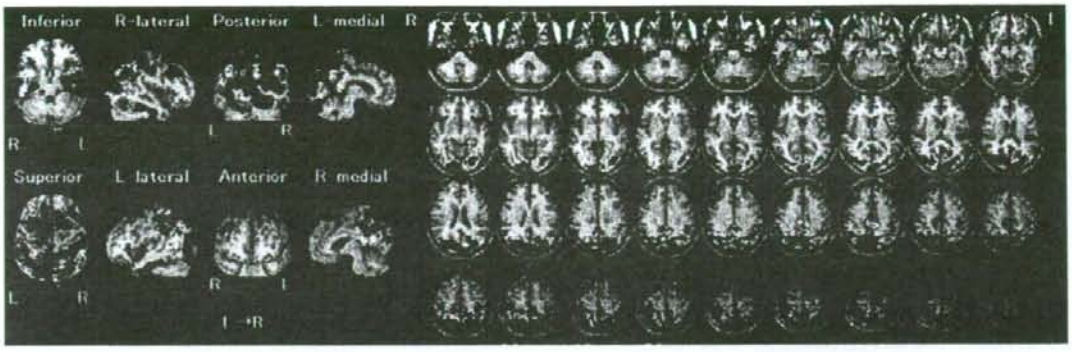

Fig. 1. A 72-year-old male AD patient with an 18-month disease duration had decreased rCBF in an area extending from the posterior cingulate cortex to the precuneus and the parietal cortex. The specific VOI analysis showed a severity index of 2.27 (>1.19), an extent of 56.63% (>14.2%) and an rCBF ratio of 4.04 (>2.22), with all three indices over the threshold set for differentiation of AD.

ticular criteria for each disease [13–16]. In addition to these clinical investigations, the diagnosis of DLB was confirmed based on the results of ^{123}I-MIBG myocardial scintigraphy, since Suzuki et al. [17] and Yoshita et al. [18] found that myocardial ^{123}I-MIBG uptake was impaired in early-stage DLB.

None of the patients had taken any medication, including donepezil, until brain perfusion SPECT was performed.

Brain SPECT Procedure

An intravenous line was established in all subjects before SPECT imaging was performed. While lying supine with eyes closed in a dimly lit quiet room, each subject received an intravenous injection of 600 MBq of ^{99m}Tc-ECD. Ten minutes after this injection, brain SPECT was performed with a double-headed gamma camera (E.CAM; Siemens, Hoffman Estates, Ill., USA) equipped with low-energy and high-resolution parallel-hole collimators. For each camera, projection data were obtained in a 128 × 128 matrix through 360° rotation at steps of 2.8° for 20 s per view. Filtered back-projection using a Butterworth and Ramp filter was used for SPECT image reconstruction.

SPECT Image Analysis using eZIS

SPECT images of all patients and all diseases were standardized anatomically with an original ^{99m}Tc-ECD template using eZIS. An averaged SPECT image for each disease was then created from these anatomically standardized images. A Z-score map for the averaged SPECT image for each disease was obtained by comparing SPECT images of age-matched healthy volunteers with the mean and standard deviation for each voxel obtained after anatomical standardization and voxel normalization to global mean values using the following equation: Z-score = ([control mean] – [individual value])/(control SD). The Z-score maps were displayed by overlay onto topographic sections and projection, with an averaged Z-score obtained from a depth of 14 mm to the surface through rendering of an anatomically standardized MRI template.

Three indicators were used for characterizing the rCBF. Decreases using a Z-score in the VOI, which was defined as the region related to AD in early AD, were automatically determined as follows. First, the severity of the decrease in rCBF in the specific region showing a decrease in rCBF in early AD was obtained from the averaged positive Z-score in the VOI. Second, the extent of the region showing a significant decrease in rCBF in the VOI was obtained; that is, the percentage of coordinates with a Z-score exceeding the threshold value of 2.0 was determined. Third, the ratio for each region showing a significant decrease in rCBF in the VOI relative to the region showing a significant decrease in rCBF in the whole brain was obtained; this ratio (rCBF ratio) indicates the specificity of the decrease in rCBF in the VOI compared with the whole brain. According to Matsuda et al. [8], the accuracies of severity, extent and the rCBF ratio in discriminating between healthy controls and patients with early AD are 85, 86, and 80%, respectively, based on cutoff values of 1.19, 14.2%, and 2.22, respectively.

Results

Images from patients obtained using eZIS showing specific VOIs for AD, VD + AD, VD, DLB and FTD are shown in figures 1–5 as clinical heuristic cases, which were chosen as prototypical of the conditions they represent.

A Mini-Mental State Examination (MMSE) score of 22.0 was determined for a 72-year-old man with AD whose disease duration was 18 months. A significant decrease in rCBF was found in the area extending from the posterior cingulate cortex to the precuneus and the parietal cortex. The specific VOI analysis of this case gave

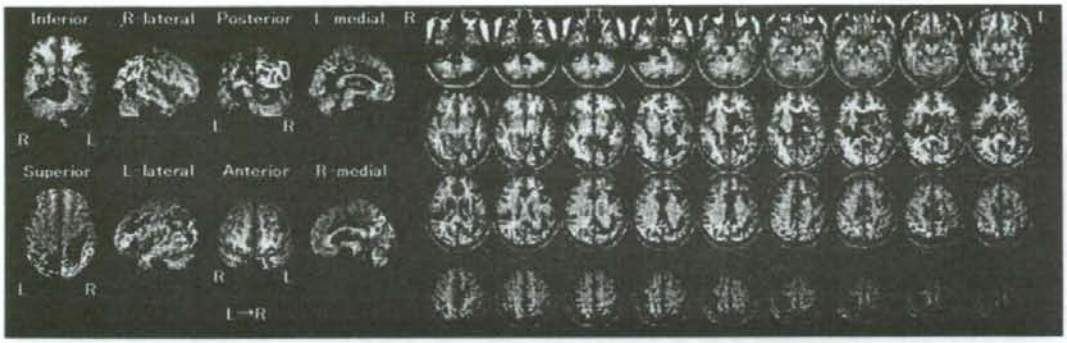

Fig. 2. An 80-year-old male VD patient with a 36-month disease duration had decreased rCBF in the basal ganglia, thalamus, posterior cortex and the cingulate cortex. The severity index, extent and rCBF ratio were 1.67 (>1.19), 20.36% (>14.2%) and 1.33 (<2.22), respectively.

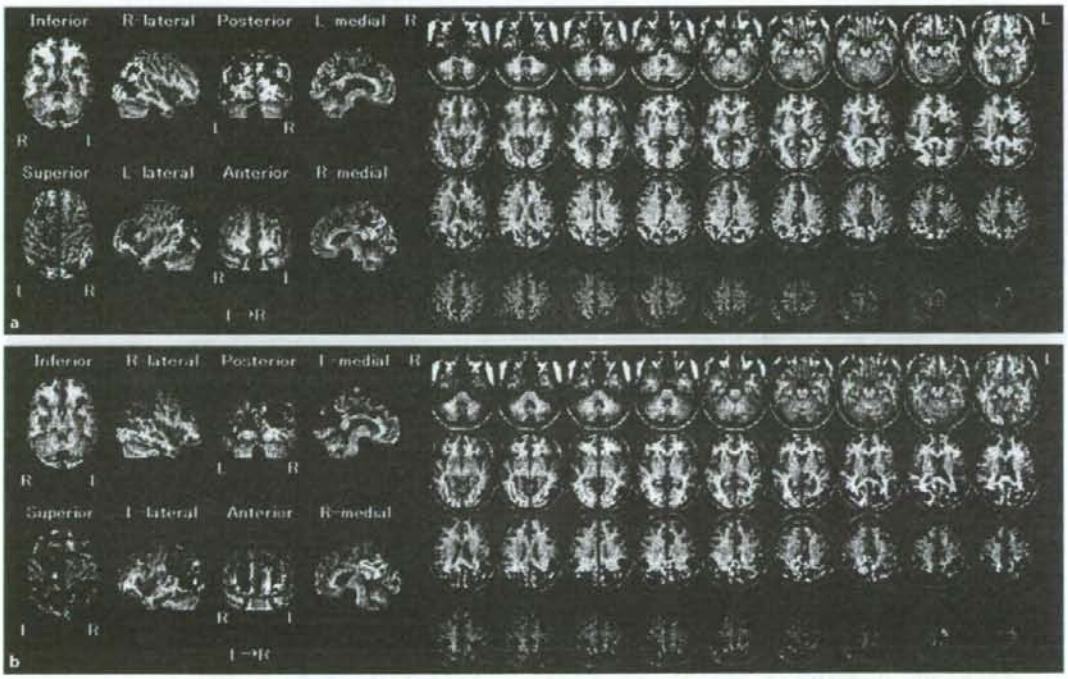

Fig. 3. An 82-year-old male patient who developed VD + AD after a stroke exhibited severely decreased rCBF in the left parietal cortex and mild reduction in the posterior cingulate gryus and parieto-occipital area. The severity index, extent and rCBF ratio were 1.55 (<1.19), 24.78% (<14.2%) and 2.86 (<2.22), respectively, at the onset of stroke (**a**). After 36 months from onset of stroke, the decreased rCBF extended to an area from the posterior cingulate cortex to the precuneus and the parietal cortex, a specific pattern for AD in which the severity index, extent and rCBF ratio were 2.25 (>1.19), 49.47% (>14.2%) and 3.66 (>2.22), respectively, with all three indicators over the threshold for discrimination of AD (**b**).

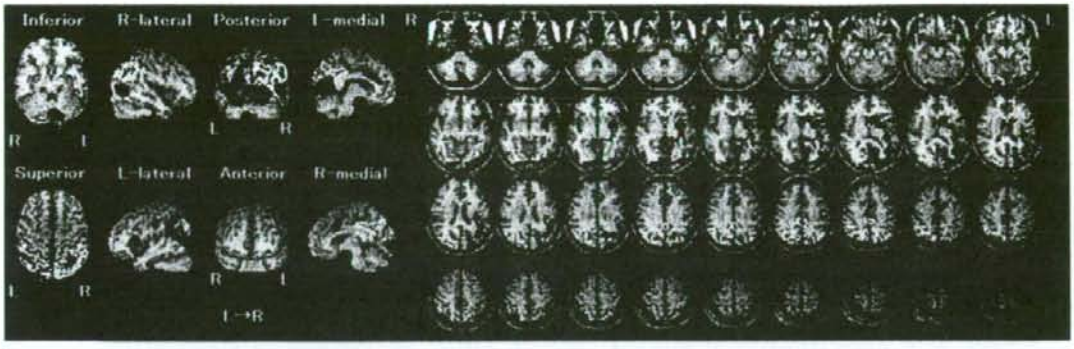

Fig. 4. A 70-year-old male with DLB and a disease duration of 12 months exhibited a decreased rCBF in the posterior cortex and the parietal cortex. The severity index, extent and rCBF ratio were 1.18 (<1.19), 11.78% (<14.2%) and 1.46 (<2.22), respectively.

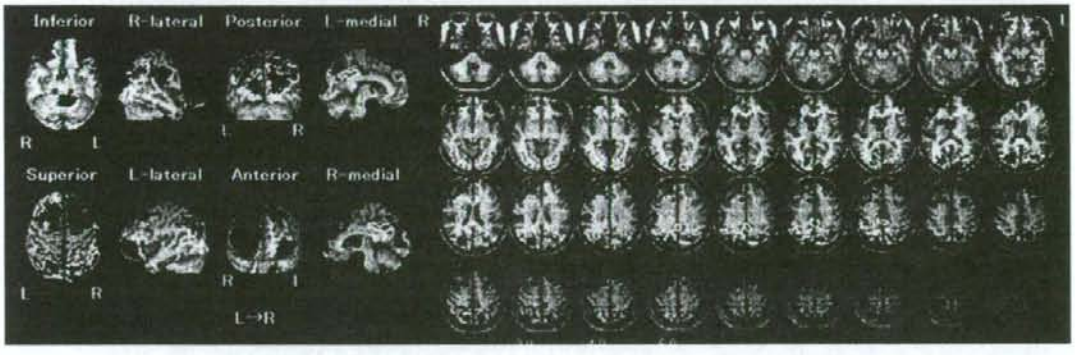

Fig. 5. A 73-year-old female with FTD with a disease duration of 12 months exhibited a decreased rCBF area in the parietal cortex and significant reduction in the frontal cortex activity. The severity index, extent and rCBF ratio were 1.43 (<1.19), 19.9% (<14.2%) and 1.90 (<2.22), respectively, with only the rCBF ratio being lower than the threshold.

a severity index of 2.27 (>1.19), an extent of 56.63% (>14.2%) and an rCBF ratio of 4.04 (>2.22), with the values of all three indicators above the cutoff value for discrimination of AD (fig. 1).

For an 80-year-old man with VD and a disease duration of 36 months, the MMSE score was 22.0. Decreased rCBF was seen in the basal ganglia, thalamus, posterior cortex and cingulate cortex; the severity index, extent and rCBF ratio were 1.67 (>1.19), 20.36% (>14.2%) and 1.33 (<2.22), respectively (fig. 2).

An 82-year-old man with VD + AD, whose disease duration was 36 months from onset of stroke, had an MMSE score of 23. At the onset of stroke, severely decreased rCBF in the left parietal cortex and a slight decrease in the posterior cingulate gyrus and parieto-occipital area were observed, with a severity index, an extent and an rCBF ratio of 1.55 (<1.19), 24.78% (<14.2%) and 2.86 (<2.22), respectively, at this stage (fig. 3a). After 36 months from onset of stroke, the decreased rCBF extended from the posterior cingulate cortex to the precuneus and parietal cortex, a specific pattern for AD. The MMSE score decreased to 18 and the severity index, extent and rCBF ratio changed to 2.25 (>1.19), 49.47% (>14.2%) and 3.66 (>2.22), respectively, with the values of

Table 2. Results of the values of three indices obtained by eZIS analysis in each dementing disease

	Severity (>1.19)			Extent (>14.2%)			rCFF ratio (>2.22)		
	range	median	average ± SD	range	median	average ± SD	range	median	average ± SD
AD	0.72–3.94	1.66	1.82 ± 0.53	1.64–92.89	25.68	30.19 ± 20.28	0.34–7.52	2.56	1.83 ± 1.12
VD + AD	1.08–3.20	1.67	1.62 ± 0.59	8.16–49.39	23.64	21.79 ± 13.36	0.77–5.39	2.14	1.83 ± 1.12
DLB	0.95–2.89	1.44	1.65 ± 0.53	5.98–60.79	21.04	21.04 ± 19.65	0.63–5.01	1.98	2.01 ± 1.19
VD	0.65–2.65	1.12	1.23 ± 0.40	0.88–44.64	16.79	16.79 ± 11.10	0.06–4.19	1.29	1.48 ± 1.07
FTD	0.69–1.62	1.04	1.09 ± 0.29	0.46–21.5	8.64	8.64 ± 6.04	0.1–1.65	0.64	0.80 ± 0.64
Normal	0.27–1.64	0.84	0.86 ± 0.28	0.6–19.27	4.64	4.64 ± 4.01	0.15–1.89	1.13	1.03 ± 0.52

all three indicators above the threshold for discrimination of AD (fig. 3b).

In a 70-year-old man with DLB, whose disease duration was 12 months from the onset of symptoms, the MMSE score was 21. A significant decrease in rCBF was found in the posterior cortex and the parietal cortex. The automated analysis resulted in a severity index of 1.18 (<1.19), an extent of 11.78% (<14.2%) and an rCBF ratio of 1.46 (<2.22) (fig. 4).

In a 73-year-old woman with FTD, whose disease duration was 12 months from the onset of symptoms, the MMSE score was 20, with some decrease in rCBF in the parietal cortex and severe reduction in the frontal cortex. In this case, severity index, extent and rCBF ratio were 1.43 (<1.19), 19.9% (<14.2%) and 1.90 (<2.22), respectively, with only the rCBF ratio being lower than the threshold value (fig. 5).

Table 2 shows the values of three indices obtained by eZIS analysis in each form of dementia. The median, mean and SD (in parentheses) for the severity of the decrease in rCBF (cutoff value 1.19) was 1.66 and 1.82 (0.53) for AD, 1.67 and 1.62 (0.59) for VD + AD, 1.44 and 1.65 (0.53) for DLB: 1.12 and 1.23 (0.40) for VD, 1.04 and 1.09 (0.29) for FTD, and 0.84 and 0.86 (0.28) for controls. The severity index in early AD was statistically higher than that for VD ($p < 0.05$), FTD and controls ($p < 0.01$). The median, mean and SD for extent of rCBF decrease (cutoff value 14.2%) was 25.68 and 30.19 (20.28) for AD, 23.64 and 21.79 (13.36) for VD + AD, 19.2 and 21.04 (19.65) for DLB: 13.08 and 16.79 (11.10) for VD, 7.43 and 8.64 (6.04) for FTD, and 3.62 and 4.64 (4.01) for controls. The extent of rCBF in early AD was statistically greater than that of FTD and controls ($p < 0.01$). The median and SD of the rCBF ratio (cutoff value 2.22) was 2.56 and 1.83 (1.12) for AD, 2.14 and 1.83 (1.12) for VD + AD, 1.98 and 2.01 (1.19) for DLB, 1.29 and 1.48 (1.07) for VD, 0.64 and 0.80 (0.64) for FTD and 1.13 and 1.03 (0.52) for controls.

The rCBF ratio in early AD was statistically higher than in VD, FTD and controls ($p < 0.01$). The rCBF ratios of all patients with VD, FTD and controls were below the cutoff value of 2.22 for early AD. Thus, the rCBF ratio might be a more sensitive marker than severity or extent of decrease in rCBF for discrimining early AD from other early-onset dementias. However, early-stage VD + AD and DLB could not be clearly discriminated from early AD by any of the three indices (table 2, fig. 6a–c).

Discussion

Matsuda et al. [8] showed that automated analysis of brain perfusion SPECT using eZIS with incorporation of specific VOI related to early AD was useful in discriminating early AD patients from age-matched healthy controls. Three indices for characterizing rCBF, i.e. severity, extent and rCBF ratio in early AD, were evaluated for discrimination of early AD from other kinds of dementia [8], and the extent of the decrease in rCBF was found to be more sensitive than the severity index and rCBF ratio when comparing patients with early AD and healthy volunteers [8]. The authors also raised the possibility that the rCBF ratio might be useful for differentiating early AD from other types of dementia [8]. In this study we thus evaluated brain perfusion SPECT for differentiating early AD from other types of early dementia, including VD with AD, DLB, VD and FTD, using an automated program with statistical analysis developed by Matsuda et al. [8].

Decreased rCBF in the posterior cingulate gyrus and the precuneus is highly specific to early AD [8–12]. DLB is characterized by recurrent visual hallucinations, fluctuating cognitive impairment, and parkinsonism [16]. As recognized in AD, which shows bilateral parietotemporal dysfunction, DLB is associated with severe occipital hy-

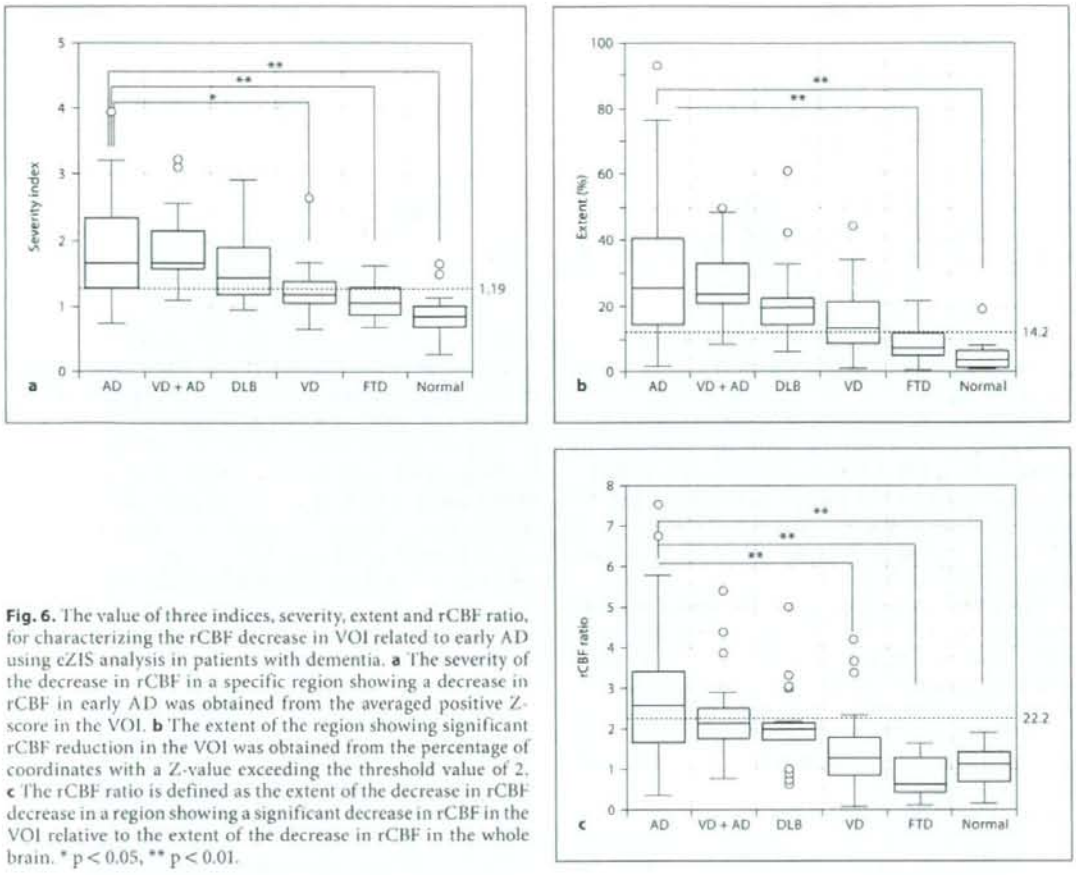

Fig. 6. The value of three indices, severity, extent and rCBF ratio, for characterizing the rCBF decrease in VOI related to early AD using eZIS analysis in patients with dementia. **a** The severity of the decrease in rCBF in a specific region showing a decrease in rCBF in early AD was obtained from the averaged positive Z-score in the VOI. **b** The extent of the region showing significant rCBF reduction in the VOI was obtained from the percentage of coordinates with a Z-value exceeding the threshold value of 2. **c** The rCBF ratio is defined as the extent of the decrease in rCBF decrease in a region showing a significant decrease in rCBF in the VOI relative to the extent of the decrease in rCBF in the whole brain. * $p < 0.05$, ** $p < 0.01$.

pometabolism and hypoperfusion in PET and SPECT images [19, 20]. All DLB patients in the current study had visual hallucinations and mild cognitive impairment as initial symptoms, and eZIS analysis showed decreases in rCBF extending from the bilateral precuneus gyrus to the partial cortex, occipital cortex, primary visual cortex and posterior cingulated cortex. These findings seem to be compatible with neurodegenerative changes in DLB. Minoshima et al. [21] reported high sensitivity (90%) and specificity (80%) in discriminating AD from DLB based on hypometabolism in the occipital cortex. The differential diagnosis between AD and DLB, in which decreased rCBF of the occipital lobe is not prominent at a very early stage, is not easy because reduced rCBF of the posterior cingulate cortex has been observed both in DLB and AD from a very early stage, as shown in our previous reports [10, 22, 23]. In such cases, brain perfusion SPECT using eZIS combined with ^{123}I-MIBG myocardial scintigraphy should be very useful for the differential diagnosis between early DLB and AD [17, 18].

FTD is the third most common neurodegenerative dementia after AD and DLB. The most common and early symptom of FTD is a decline in social interpersonal behavior [15]. Functional neuroimaging studies using SPECT or PET may be helpful for diagnosis because early-stage FTD is sometimes misdiagnosed as AD, manic-depressive illness and schizophrenia [24]. SPECT or PET images show hypoperfusion of the anterior cerebral cor-

tex with relative sparing of the posterior cortex in FTD patients [25]; using SPECT with eZIS we were able to demonstrate decreased rCBF in the frontal cortex, temporal cortex and the orbitofrontal cortex. These regions are related to antisocial behavioral symptoms in patients with FTD [24]. Bonte et al. [26] emphasized the presence of a decrease in rCBF in the posterior cingulate gyrus (posterior cingulate sign) for differentiating AD from FTD. Sixteen of 20 AD patients showed posterior cingulate signs whereas only 1 of 20 FTD patients showed this sign [26].

In summary, in this study, three indices of early AD were characterized by automated analysis of brain perfusion SPECT using eZIS and VOI: severity, extent and rCBF ratio. This method appears to be helpful in discriminating early AD from other types of dementia. Our results suggest that the rCBF ratio may be useful in differentiating early AD from other types of dementia and confirm the hypothesis of Matsuda et al. [8]. DLB may be discriminated from AD based on clinical signs such as parkinsonism and impaired myocardial ^{123}I-MIBG findings [17, 18], whereas the clinical discrimination between AD and AD + VD (mixed dementia) may be more difficult because similar dementias share similar vascular pathology [14, 27, 28].

Our results show that the values of three indices, and especially the rCBF ratio, in brain perfusion SPECT using eZIS with incorporation of AD-specific VOI may be useful for discriminating AD from other types of dementia as an adjunct to the early diagnosis of patients with dementia. In addition, we resolved some of the limitations of current methods for discriminating early AD from other types of dementia using statistical analysis of brain perfusion SPECT. The statistical approach of brain perfusion SPECT using eZIS combined with a clinical evaluation using MMSE, Alzheimer's Disease Assessment Scale-cognitive subscale, Clinical Dementia Rating and other neuroimaging methods will be powerful for early diagnosis and monitoring of disease progression as well as for accurate and objective evaluation of therapeutic effects in patients with dementia.

Follow-up studies will be needed in each individual case to confirm specific patterns as shown in this study.

Acknowledgement

We thank Hiroshi Tazumi and Hiroyuki Saeki (Fujifilm RI Pharma, Ltd. Tokyo, Japan) for their technical advice and support.

References

1 Ashburner J, Friston KJ: Voxel-based morphometry - the methods. Neuroimage 2000; 11:805–821.
2 Frith CD, Friston KJ, Ashburner J, et al: Principles and methods; in Frackowiak RSJ, Friston KJ, Frith CD, Dolan RJ, Mazziotta JC (eds): Human Brain Function, ed 1. San Diego, Academic Press, 1997, pp 3–159.
3 Minoshima S, Berger KL, Lee KS, et al: An automated method for rotational correction and centering of three-dimensional functional brain images. J Nucl Med 1992;33: 1579–1585.
4 Minoshima S, Koeppe RA, Mintun MA, et al: Automated detection of the intercommissural line for stereotactic localization of functional brain images. J Nucl Med 1993; 34:322–329.
5 Minoshima S, Koeppe RA, Frey KA, et al: Anatomic standardization: linear scaling and nonlinear warping of functional brain images. J Nucl Med 1994 ;35:1528–1537.
6 Matsuda H, Mizumura S, Soma T, et al: Conversion of brain SPECT images between different collimators and reconstruction processes for analysis using statistical parametric mapping. Nucl Med Commun 2004; 25:67–74.
7 Kanetaka H, Matsuda H, Asada T, et al: Effects of partial volume correction on discrimination between very early Alzheimer's dementia and controls using brain perfusion SPECT. Eur J Nucl Med Mol Imaging 2004; 31:975–980.
8 Matsuda H, Mizumura S, Nagao T, et al: Automated discrimination between very early Alzheimer's disease and controls using an easy Z-score imaging system for multicenter brain perfusion SPECT. AJNR Am J Neuroradiol 2007;28:731–736.
9 Matsuda H: Role of neuroimaging in Alzheimer's disease, with emphasis on brain perfusion SPECT. J Nucl Med 2007;48:1289–1300.
10 Waragai M, Yamada T, Matsuda H: Evaluation of brain perfusion SPECT using an easy Z-score imaging system (eZIS) as an adjunct to early diagnosis of neurodegenerative diseases. J Neurol Sci 2007;260:57–64.
11 Johnson KA, Jones K, Holman BL, et al: Preclinical prediction of Alzheimer's disease using SPECT. Neurology 1998;50:1563–1571.
12 Kogure D, Matsuda H, Ohnishi T, et al: Longitudinal evaluation of early Alzheimer's disease using brain perfusion SPECT. J Nucl Med 2000;41:1155–1162.
13 McKhann G, Drachman D, Folstein M, et al: Clinical diagnosis of Alzheimer's disease: report of the NINCDS-ADRDA Work Group under the auspices of Department of Health and Human Services Task Force on Alzheimer's Disease. Neurology 1984;34:939–944.
14 Román GC, Tatemichi TK, Erkinjuntti T, et al: Vascular dementia: diagnostic criteria for research studies. Report of the NINDS-AIREN International Workshop. Neurology 1993;43:250–260.
15 Rosen HJ, Hartikainen KM, Jagust W, et al: Utility of clinical criteria in differentiating frontotemporal lobar degeneration (FTLD) from AD. Neurology 2002;58:1608–1615.
16 McKeith IG, Dickson DW, Lowe J, et al: Diagnosis and management of dementia with Lewy bodies: third report of the DLB Consortium. Neurology 2005;65:1863–1872.

17 Suzuki M, Kurita A, Hashimoto M, et al: Impaired myocardial ^{123}I-metaiodobenzylguanidine uptake in Lewy body disease: comparison between dementia with Lewy bodies and Parkinson's disease. J Neurol Sci 2006; 240:15–19.
18 Yoshita M, Taki J, Yokoyama K, et al: Value of ^{123}I-MIBG radioactivity in the differential diagnosis of DLB from AD. Neurology 2006; 66:1850–1854.
19 Minoshima S, Giordani B, Berent S, et al: Metabolic reduction in the posterior cingulate cortex in very early Alzheimer's disease. Ann Neurol 1997;42:85–94
20 Ishii K, Imamura T, Sasaki M, et al: Regional cerebral glucose metabolism in dementia with Lewy bodies and Alzheimer's disease. Neurology 1998;51:125–130.
21 Lobotesis K, Fenwick JD, Phipps A, et al: Occipital hypoperfusion on SPECT in dementia with Lewy bodies but not AD. Neurology 2001;56:643–649.
22 Minoshima S, Foster NL, Sima AA, et al: Alzheimer's disease versus dementia with Lewy bodies: cerebral metabolic distinction with autopsy confirmation. Ann Neurol 2001;50:358–365.
23 Shimizu S, Hanyu H, Kanetaka H, et al: Differentiation of dementia with Lewy bodies from Alzheimer's disease using brain SPECT. Dement Geriatr Cogn Disord 2005;20:25–30.
24 Nakano S, Asada T, Yamashita F, et al: Relationship between antisocial behavior and regional cerebral blood flow in frontotemporal dementia. Neuroimage 2006;32:301–306.
25 Charpentier P, Lavenu I, Defebvre L, et al: Alzheimer's disease and frontotemporal dementia are differentiated by discriminant analysis applied to ^{99m}Tc HmPAO SPECT data. J Neurol Neurosurg Psychiatry 2000; 69:661–663.
26 Bonte FJ, Harris TS, Roney CA, et al: Differential diagnosis between Alzheimer's and frontotemporal disease by the posterior cingulate sign. J Nucl Med 2004;45:771–774.
27 Irie F, Fitzpatrick AL, Lopez OL, et al: Enhanced risk for Alzheimer disease in persons with type 2 diabetes and APOE ε4: the Cardiovascular Health Study Cognition Study. Arch Neurol 2008;65:89–93.
28 Gold G, Giannakopoulos P, Herrmann FR, et al: Identification of Alzheimer and vascular lesion thresholds for mixed dementia. Brain 2007;130:2830–2836.

Ann Nucl Med (2008) 22:921–927
DOI 10.1007/s12149-008-0211-7

ORIGINAL ARTICLE

Comparison of SPM and NEUROSTAT in voxelwise statistical analysis of brain SPECT and MRI at the early stage of Alzheimer's disease

Masaki Nishimiya · Hiroshi Matsuda
Etsuko Imabayashi · Ichiei Kuji · Noriko Sato

Received: 9 September 2008 / Accepted: 26 September 2008

Abstract
Objective Neuroimaging plays a major role in the early diagnosis of Alzheimer's disease (AD). Recent advances in voxelwise statistical analysis after anatomic standardization of images have made this early diagnosis easier and more objective than visual inspection. We present comparative observations of NEUROSTAT, statistical parametric mapping (SPM) 99, and SPM2 in the early diagnosis of AD using brain perfusion single-photon emission computed tomography (SPECT) and magnetic resonance imaging (MRI).
Methods We performed voxel-by-voxel statistical group analysis for brain perfusion SPECT and gray matter images segmented from MRI between 61 patients with very early AD and 82 age-matched healthy volunteers. Anatomic standardization was performed using NEUROSTAT, SPM99, and SPM2 using both original and common templates.
Results The location of significant reduction of regional cerebral blood flow (rCBF) for SPECT and gray matter concentration for MRI were identical among these three methods irrespective of the templates used. When using the original template, the significance of peak rCBF reduction in the posterior cingulate gyri was higher in SPM99 and SPM2 than that in NEUROSTAT. On the other hand, when using the common template, the significance of peak rCBF reduction in the posterior cingulate gyri was higher in NEUROSTAT and SPM2 than that in SPM99. NEUROSTAT showed almost the equal significance of peak rCBF reduction between the used templates. Almost the equal significance of reduction in gray matter concentration was observed in the parahippocampal gyri among the three methods.
Conclusions NEUROSTAT, SPM99, and SPM2 showed identical location of significant reductions in rCBF and gray matter concentration in very early AD patients. Used templates for anatomic standardization are relevant to the results of voxelwise statistical analysis in SPM, less prominently in SPM2 than in SPM99, whereas irrelevant in NEUROSTAT.

Keywords SPM · NEUROSTAT · Alzheimer's disease · SPECT · MRI

M. Nishimiya · H. Matsuda (✉) · E. Imabayashi · I. Kuji
Department of Nuclear Medicine, Saitama Medical University International Medical Center, 1397-1 Yamane, Hidaka, Saitama 350-1298, Japan
e-mail: matsudah@saitama-med.ac.jp

H. Matsuda · E. Imabayashi · N. Sato
Department of Radiology, National Center Hospital for Mental, Nervous, and Muscular Disorders, National Center of Neurology and Psychiatry, Kodaira, Tokyo, Japan

Introduction

Developments in the diagnosis and treatment of age-related cognitive decline have led to better detection and symptomatic treatment of Alzheimer's disease (AD), and both structural and functional brain neuroimaging is often used to assist physicians in making an early and accurate diagnosis. At a very early stage of AD, even before a clinical diagnosis of probable AD is possible, decreases in glucose metabolism or regional cerebral blood flow (rCBF) in the posterior cingulate gyri and precunei have been reported using positron emission tomography (PET) or single-photon emission computed tomography (SPECT) [1, 2]. Moreover, many structural magnetic resonance imaging (MRI) studies have

demonstrated that atrophy of the medial temporal lobe, such as hippocampus and entorhinal cortex, is a sensitive marker of early AD [3, 4]. However, it is difficult to distinguish a slight decrease of rCBF or metabolic activity in the posterior cingulate gyri and precunei and evaluate slight atrophy of medial temporal structures in subjects with early AD by visual inspection. Recent advances in computer-assisted evaluation of functional and morphological images using voxelwise statistical analysis have made it easier to detect these regional slight changes. For intersubject comparisons on a voxel-by-voxel basis, individual brain images need to be transformed into a standard coordinate system, such as that proposed by Talairach and Tournoux [5], to compensate for individual variability in size and shape. The results of voxelwise statistical analysis depend considerably on the precision of this anatomic standardization. Two commonly used anatomic standardization techniques, statistical parametric mapping (SPM, The Wellcome Department of Neurology, London, UK) [6] and NEUROSTAT (Department of Internal Medicine, University of Michigan, Ann Arbor, MI, USA) [7, 8], have been developed and used at various institutions for both research and clinical studies. In a comparative study between these two techniques, no differences in the precision of anatomic standardization were found in healthy normal subjects [9]. On the other hand, NEUROSTAT has been reported to be less affected by the presence of atrophy than SPM99 in patients with AD [10]. However, this comparison was done only with SPM99 and NEUROSTAT for ^{18}F-fluorodeoxyglucose (FDG) PET images. Now a newer version, SPM2 is commonly used and believed to be more accurate than SPM99 for anatomic standardization. The objective of this study was to compare the findings of NEUROSTAT, SPM99, and SPM2 in voxel-by-voxel statistical group analysis for brain perfusion SPECT and MRI between early AD patients and age-matched healthy volunteers.

Materials and methods

Subjects

We retrospectively chose 61 patients (32 men and 29 women) with a clinical diagnosis of probable AD according to the National Institute of Neurological and Communicative Disorders and Stroke and the Alzheimer's Disease and Related Disorders Association criteria (NINCDS-ADRDA) [11]. At the initial visit, they showed verbal and/or visual episodic memory impairment in delayed recall, as defined by performance 1.5 standard deviation (SD) below the mean for age-matched normal controls in learning a list of 10 words, 15-item story recall test, and Rey–Osterrieth complex figure test. These neuropsychologic tests were performed by well-trained clinical psychologists. They had no apparent loss in general cognitive, behavioral, or functional status and corresponded to the criteria of the amnestic type of mild cognitive impairment as proposed by Petersen et al. [12]. Their age ranged from 48 years to 87 years with a mean ± SD, 70.6 ± 8.4. The Mini-Mental State Examination (MMSE) score ranged from 24 to 29; 26.0 ± 1.5 at the initial visit. During the subsequent follow-up period of 2–6 years, the subjects showed progressive cognitive decline and eventually fulfilled the diagnosis of probable AD according to the NINCDS-ADRDA.

Eighty-two control subjects (39 men and 43 women, age 54–86 years, mean 70.1, SD 7.7) were healthy volunteers with no memory impairment or cognitive disorders. Their performance was within normal limits both on the Wechsler Memory Scale-Revised and Wechsler Adult Intelligence Scale-Revised. The MMSE score ranged from 26 to 30; 28.7 ± 1.5. They did not differ significantly in age or the number of formal years of education from the AD patients.

The Ethics Committee of the National Center of Neurology and Psychiatry approved this study for healthy volunteers and AD patients, all of whom provided informed consent to participate. All the subjects were right-handed and screened by questionnaire and medical history to exclude those with medical conditions potentially affecting the central nervous system. In addition, none of them had asymptomatic cerebral infarction detected by T2-weighted MRI.

MRI data

All MRI studies were performed on a 1.0-T system (Magnetom Impact Expert; Siemens, Erlangen, Germany). A three-dimensional volumetric acquisition produced a gapless series of thin sagittal sections using a Magnetization Prepared Rapid Gradient Echo sequence (echo time/repetition time/inversion time, 4.4/11.4/300 ms; flip angle 15°, acquisition matrix 256 × 256; 1 excitation; field of view 31.5 cm; slice thickness 1.23 mm). Gray matter images were segmented from these MRI using SPM2 software installed on a Windows XP machine for further analysis using voxel-based morphometry [13].

SPECT data

Each subject received an intravenous injection of 600 MBq of ^{99m}Tc-ethyl cysteinate dimer (ECD) when lying down in the supine position with eyes closed in a

dimly lit, quiet room. Ten minutes after the injection of the tracer, brain SPECT was performed using triple-head rotating γ-cameras (Multispect3; Siemens Medical Systems) equipped with high-resolution fanbeam collimators. For each camera, projection data were obtained in a 128 × 128 format for 24 angles of 120° at 50 s per angle. A Shepp and Logan Hanning filter was used for SPECT image reconstruction at 0.7 cycle/cm. Attenuation correction was performed using Chang's method.

Anatomic standardization

NEUROSTAT

A NEUROSTAT software was installed on a Windows XP machine. In an anatomic standardization algorithm, an individual brain image set was first aligned to the midsagittal plane. The AC–PC line (a line passing through the anterior and posterior commissures) was estimated by iterative matching between the individual image set and a standard atlas template. This standard atlas template was produced as an average of FDG images from 66 healthy volunteers. The template was created using a nonlinear stereotactic deformation method. The right hemisphere was inverted and copied to the left hemisphere to make the template symmetric. The individual image set was realigned to the standard stereotactic coordinate system on the basis of the estimated AC–PC line. Differences in size between the individual brain and the standard template were removed by linear scaling. For this process, nine affine transformation parameters were estimated. To adjust the individual brain shape to the stereotactic atlas coordinate system proposed by Talrairach and Tournoux, nonlinear warping along the directions of major neuronal fiber bundles within the brain was performed. The directions were predefined in the stereotactic coordinate space on the basis of the fiber origins and their cortical projections. Individual landmarks for cortical projections were searched iteratively between centers and cortical landmarks predetermined on the template brain using a profile curve analysis. Detected individual landmarks were then warped to predefined landmarks, resulting in a standardized image set with a uniform voxel size of 2.25 mm, interpolation to 60 slices and a matrix size for 128 × 128. For the common use of the SPECT and MRI templates between SPM and NEUROSTAT, the ECD SPM template previously developed by us [14] and the gray matter SPM template supplied as a priori gray matter image were anatomically standardized by NEUROSTAT with an original NEUROSTAT FDG template. Anatomic standardization of SPECT and MRI for early AD patients and healthy volunteers was performed with these common ECD and gray matter templates, respectively. Additionally, anatomic standardization was also performed with the original NEUROSTAT FDG template for SPECT.

SPM

SPM99 and SPM2 software programs were installed on a Windows XP machine. Calculations and image matrix manipulations were performed in MATLAB 5.3 for SPM99 and MATLAB6.5 for SPM2 (The MathWorks, Natick, MA, USA). The first step of the normalization was to determine the optimum 12-parameter affine transformation. This step has been made more reliable by making the procedure more internally consistent in SPM2 than in SPM99. Next, nonlinear deformation of individual brain shape was performed by a linear combination of three-dimensional discrete cosine transform basis functions. Matching involved simultaneous minimization of membrane energies from the deformation fields and the residual squared difference between the images and templates. For anatomic standardization, the number of nonlinear basis functions was set to 7 × 8 × 7 for SPM99 and 7 × 9 × 7 for SPM2, the number of iterations to 12 for SPM99 and 16 for SPM2, and the nonlinear regularization to medium. Other parameters for anatomically standardized image set output were as follows: bounding box, −90:90, −126:90, −72:108; voxel sizes 2 × 2 × 2 mm; image size 91 × 109 × 91; and origin (46, 64, 37). Anatomic standardization was performed with the common ECD template for SPECT and the common gray matter template for MRI. When the common ECD and gray matter templates were used, the bounding box was set to −141.75:145.25 −157.5:129.50 −60.75:73.25, voxel sizes were 2.25 × 2.25 × 2.25 mm, image size was 128 × 128 × 60, and origin was (64, 71, 28). Additionally, anatomic standardization was also performed with the original SPM ECD template for SPECT. In this case, we used the original bounding box, voxel size, and origin of SPM.

Statistical image analysis

All the anatomically standardized SPECT and gray matter images were smoothed with Gaussian kernel 12 mm in full width at half maximum. The processed images were statistically analyzed using SPM99, which implemented a general linear model. The overall mean of gray matter concentration and global cerebral blood flow was treated as a confounding covariate. A proportional scaling routine was used to achieve global normalization of voxel values between images. We studied differences in gray matter concentration and rCBF

Table 1 Location of significant decrease of regional cerebral blood flow (rCBF) in Alzheimer's disease (AD) patients as compared with normal controls when using original templates

Comparison	*k*	*t* value (Z value)	Talairach coordinates			Region
			x	*y*	*z*	
SPM99 (original ECD template)	1793	9.41 (Infinite)	0	−45	30	Posterior cingulate gyrus
	721	7.62 (6.96)	46	−62	42	Right parietal cortex
	377	6.95 (6.44)	−44	−62	42	Left parietal cortex
	140	6.36 (5.95)	−36	−17	−19	Left parahippocampal gyrus
SPM2 (original ECD template)	1778	9.49 (Infinite)	2	−45	32	Right posterior cingulate gyrus
	518	6.84 (6.34)	44	−56	40	Right parietal cortex
	247	6.69 (6.23)	−44	−60	40	Left parietal cortex
	103	6.05 (5.69)	−36	−19	−21	Left parahippocampal gyrus
NEUROSTAT (original FDG template)	1576	8.63 (7.71)	−2	−42	28	Left posterior cingulate gyrus
	340	7.28 (6.70)	−33	−18	−18	Left parahippocampal gyrus
	1057	7.27 (6.69)	40	−57	40	Right parietal cortex
	608	6.84 (6.35)	−40	−59	38	Left parietal cortex

Table 2 Location of significant decrease of rCBF in AD patients as compared with normal controls when using a common template

Comparison	*k*	*t* value (*Z* value)	Talairach coordinates			Region
			x	*y*	*z*	
SPM99 (common ECD template)	658	6.95 (6.43)	−2	−45	25	Left posterior cingulate gyrus
	249	6.40 (5.99)	42	−59	34	Right parietal cortex
	41	5.55 (5.27)	−33	−16	−16	Left parahippocampal gyrus
	53	5.43 (5.17)	−42	−62	34	Left parietal cortex
SPM2 (common ECD template)	1014	8.27 (7.45)	−4	−45	27	Left posterior cingulate gyrus
	246	6.25 (5.87)	−49	−62	32	Left parietal cortex
	308	6.19 (5.81)	38	−62	32	Right parietal cortex
	103	6.06 (5.71)	−36	−16	−16	Left parahippocampal gyrus
NEUROSTAT (common ECD template)	2910	8.44 (7.58)	−4	−44	28	Left posterior cingulate gyrus
		7.25 (6.67)	40	−57	40	Right parietal cortex
	328	7.09 (6.54)	−33	−16	−18	Left parahippocampal gyrus
	582	6.84 (6.35)	−42	−59	38	Left parietal cortex

between early AD patients and age-matched healthy volunteers using *t* statistics. The resulting sets of *t* values constituted statistical parametric maps [SPM(*t*)]. The SPM(*t*) were transformed to the unit normal distribution [SPM(*Z*)] and were subjected to a threshold of $P < 0.001$. To correct for multiple comparisons inherent in this analysis, the resulting foci were then characterized in terms of their spatial extent. This characterization is in terms of the probability that a region of the observed number of voxels, or more, could have occurred by chance over the entire volume analyzed. The significance of each region was estimated with a threshold of $P = 0.05$ using distributional approximations from the theory of Gaussian fields [6]. Anatomic localization was done according to Talairach's atlas using M. Brett's set of linear transformations (http://www.imaging.mrc-cbu.cam.ac.uk/imaging/MniTalairach).

Results

Figure 1 and Table 1 show the location and peaks of significant reduction of rCBF in early AD patients as compared with healthy volunteers when using original templates in the three methods. The rCBF was significantly reduced in the bilateral posterior cingulate gyri, parietal lobes, and left parahippocampal gyrus. As for *t* values in the posterior cingulate gyri with the most significant rCBF reduction in all methods, NEUROSTAT (8.63) showed a lower value than SPM99 (9.41) and SPM2 (9.49). The total size of all clusters increased in the order of SPM2 (2646), SPM99 (3031), and NEUROSTAT (3581).

Figure 2 and Table 2 show the location and peaks of significant reduction of rCBF in early AD patients when using common templates in the three methods. The

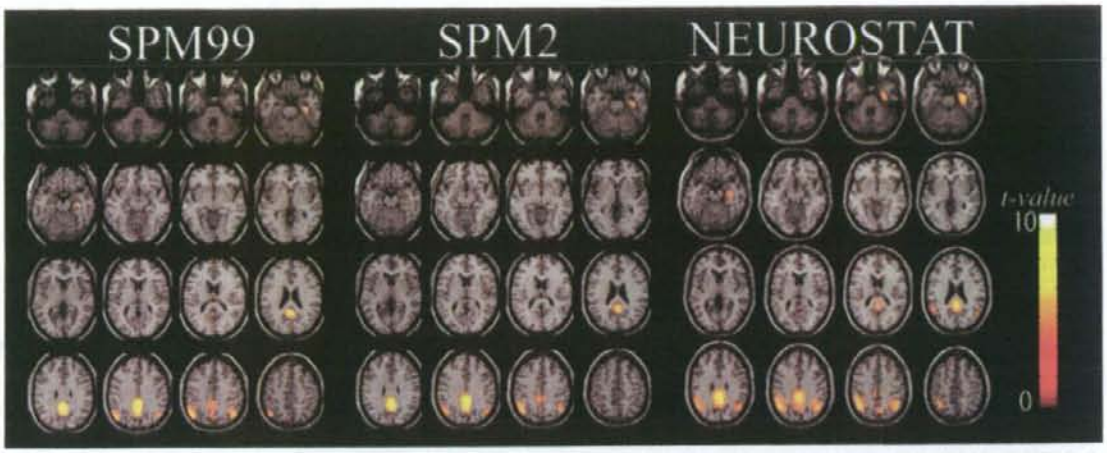

Fig. 1 Significant decrease of regional cerebral blood flow (rCBF) in Alzheimer's disease (AD) patients as compared with normal controls when using original templates in anatomic standardization using statistical parametric mapping (SPM) 99, SPM2, and NEUROSTAT

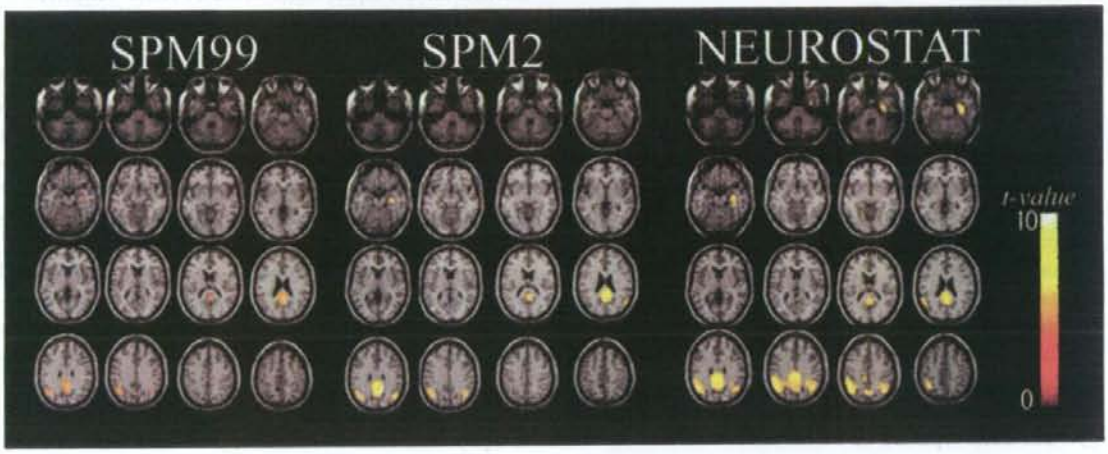

Fig. 2 Significant decrease of rCBF in AD patients as compared with normal controls when using the common ^{99m}Tc-ethyl cysteinate dimer (ECD) template in anatomic standardization using SPM99, SPM2, and NEUROSTAT

rCBF was also significantly reduced in the bilateral posterior cingulate gyri, parietal lobes, and left parahippocampal gyrus. As for *t* values in the posterior cingulate gyri with the most significant rCBF reduction in all methods, SPM99 (6.95) showed a lower value than SPM2 (8.27) and NEUROSTAT (8.44). The total size of all clusters was increased in the order of SPM99 (1001), SPM2 (1671), and NEUROSTAT (3820).

Figure 3 and Table 3 show the location and peaks of significant reductions of gray matter concentrations in early AD patients as compared with healthy volunteers when using common gray matter templates in the three methods. The gray matter concentration was significantly

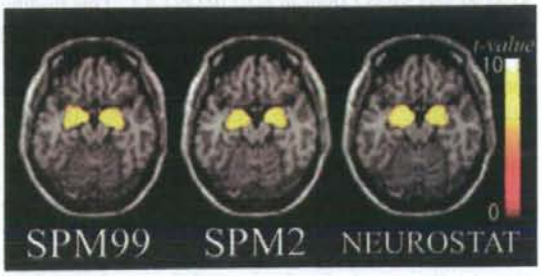

Fig. 3 Significant decrease of gray matter concentration in the AD group as compared with age-matched healthy volunteers when using the common gray matter template in anatomic standardization using SPM99, SPM2, and NEUROSTAT

Table 3 Location of significant decrease of gray matter concentration in early AD patients as compared with normal controls when using a common template

Comparison	*k*	*t* value (*Z* value)	Talairach coordinates			Region
			x	*y*	*z*	
SPM99 (common gray matter template)	542	8.53 (7.64)	−18	−5	−17	Left parahippocampal gyrus
	560	7.62 (6.96)	20	−3	−15	Right parahippocampal gyrus
SPM2 (common gray matter template)	1149	8.67 (7.74)	2	−45	32	Right parahippocampal gyrus
		8.63 (7.71)	−22	−5	−15	Left parahippocampal gyrus
NEUROSTAT (common gray matter template)	656	8.78 (7.82)	16	−5	−15	Right parahippocampal gyrus
	525	7.87 (7.15)	−20	−3	−17	Left parahippocampal gyrus

reduced in the bilateral parahippocampal gyri. The sum of *t* values in these areas was almost equal in SPM2 (17.3), NEUROSTAT (16.65), and SPM99 (16.15). The total size of all clusters was also almost equal in NEUROSTAT (1149), SPM99 (1181), and SPM2 (1102).

Discussion

We evaluated the effects of stereotactic anatomic standardization by NEUROSTAT, SPM99, and SPM2 in the application of statistical group comparisons between healthy volunteers and early AD patients. In voxel-based morphometry using gray matter images segmented from MRI, most significant reduction of gray matter concentration was equally observed in the bilateral parahippocampal gyri among the three methods. Although the location of significant rCBF reductions shown by the three methods in SPECT studies was similar in the bilateral posterior cingulate gyri, parietal cortices, and left parahippocampal gyrus, differences were seen in the significance and extent of estimated rCBF reductions. Of these areas, rCBF reduction in the posterior cingulate gyri has been reported to be the most effective for the early diagnosis of AD [15]. Using the original templates in the three methods, the significance of the rCBF reduction located in the posterior cingulate gyri was higher in SPM99 and SPM2 than in NEUROSTAT. This finding is different from that earlier reported by Ishii et al. [10] in which NEUROSTAT demonstrated higher *t* values in the area with the most significant metabolic reduction than SPM99. This may be because they used the ^{15}O–H_2O SPM template for anatomic standardization of FDG in SPM99. In contrast to purely anatomic standardization of NEUROSTAT using cortical landmarks, mathematical nonlinear basis function in anatomic standardization of SPM depends not only on the shape but also on the count distribution of the used template. Great differences in count distribution have been reported to be present in the cerebellum and medial temporal areas between ^{15}O–H_2O and FDG [16]. In the present study, an ECD template identical to the used SPECT tracer was applied in SPM.

SPM99 and SPM2 demonstrated declines in both the significance and extent of rCBF reductions when using the common ECD template instead of the original SPM ECD template. This tendency was more prominent in SPM99 than in SPM2. Even in this situation, SPM2 showed almost equal significance of rCBF reduction to NEUROSTAT in the posterior cingulate gyri, with only the image and voxel sizes differing between these two ECD templates. These results suggest that optimal parameters for anatomic standardization may vary in the template size in SPM. This variation may be more prominent in SPM99 than in SPM2. In contrast, NEUROSTAT showed almost the same *t* values and cluster sizes between the common ECD template and the original NEUROSTAT FDG template.

The extent of rCBF reductions in early AD estimated by SPM was smaller than that estimated by NEUROSTAT. However, this does not indicate simply greater sensitivity. As Ishii et al. [10] suggested, greater mismatches in anatomic standardization may result in erroneously large estimates of rCBF reductions caused by atrophy. The results indicated that the estimated extent of rCBF reductions depends on the method of anatomic standardization.

Some study limitations must be noted. First, we studied AD patients at the very early stage. Precision in anatomic standardization should be investigated in the more advanced stage with greater atrophy. However, the role of neuroimaging in AD exists in the diagnosis at the prodromal stage of mild cognitive impairment [17]. Second, the present results in brain perfusion SPECT were limited to ECD. Further investigation may be necessary for other SPECT tracers.

Conclusions

Voxelwise statistical analysis of brain perfusion SPECT using ECD and MRI in very early AD patients showed

identical location of significant reduction of rCBF and gray matter concentration among NEUROSTAT, SPM99, and SPM2. In contrast to being irrelevant to used templates in NEUROSTAT, optimization of used templates may be necessary for SPM in anatomic standardization.

Acknowledgments This work was supported by Grant-in-Aid for Scientific Research (C) 18591364. The authors thank the technical staff in our hospitals for data acquisition and Mr. John Gelblum for proofreading this manuscript.

References

1. Minoshima S, Giordani B, Berent S, Frey KA, Foster NL, Kuhl DE. Metabolic reduction in the posterior cingulate cortex in very early Alzheimer's disease. Ann Neurol 1997;42: 85–94.
2. Kogure D, Matsuda H, Ohnishi T, Asada T, Uno M, Kunihiro T, et al. Longitudinal evaluation of early Alzheimer's disease using brain perfusion SPECT. J Nucl Med 2000;41: 1155–62.
3. Chételat G, Desgranges B, De La Sayette V, Viader F, Eustache F, Baron JC. Mapping gray matter loss with voxel-based morphometry in mild cognitive impairment. Neuroreport 2002;13:1939–43.
4. Hirata Y, Matsuda H, Nemoto K, Ohnishi T, Hirao K, Yamashita F, et al. Voxel-based morphometry to discriminate early Alzheimer's disease from controls. Neurosci Lett 2005; 382:269–74.
5. Talairach J, Tournoux P. Co-planar stereotactic atlas of the human brain. Stuttgart: Thieme; 1998.
6. Frith CD, Friston KJ, Ashburner J. Principles and methods. In: Frackowiak RSJ, Friston KJ, Frith CD, Dolan RJ, Mazziotta JC, editors. Human brain function. San Diego: Academic Press; 1997. p. 3–159.
7. Minoshima S, Koeppe RA, Frey KA, Kuhl DE. Anatomic standardization: linear scaling and nonlinear warping of functional brain images. J Nucl Med 1994;35:1528–37.
8. Minoshima S, Frey KA, Koeppe RA, Foster NL, Kuhl DE. A diagnostic approach in Alzheimer's disease using three-dimensional stereotactic surface projections of fluorine-18-FDG PET. J Nucl Med 1995;36:1238–48.
9. Hosaka K, Ishii K, Sakamoto S, Sadato N, Fukuda H, Kato T, et al. Validation of anatomical standardization of FDG-PET images of normal brain: comparison of SPM and NEUROSTAT. Eur J Nucl Med Mol Imaging 2005;32:92–7.
10. Ishii K, Willoch F, Minoshima S, Drzezga A, Ficaro EP, Cross DJ, et al. Statistical brain mapping of 18F-FDG PET in Alzheimer's disease: validation of anatomic standardization for atrophied brains. J Nucl Med 2001;42:548–57.
11. McKhann G, Drachman D, Folstein M, Katzman R, Price D, Stadlan EM. Clinical diagnosis of Alzheimer's disease: report of the NINCDS-ADRDA work group under the auspices of department of health and human services task force on Alzheimer's disease. Neurology 1984;34:939–44.
12. Petersen RC, Doody R, Kurz A, Mohs RC, Morris JC, Rabins PV, et al. Current concepts in mild cognitive impairment. Arch Neurol 2001;58:1985–92.
13. Ashburner J, Friston KJ. Voxel-based morphometry: the methods. Neuroimage 2000;11:805–21.
14. Ohnishi T, Matsuda H, Hashimoto T, Kunihiro T, Nishikawa M, Uema T, et al. Abnormal regional cerebral blood flow in childhood autism. Brain 2000;123:1838–44.
15. Imabayashi E, Matsuda H, Asada T, Ohnishi T, Sakamoto S, Nakano S, et al. Superiority of 3-dimensional stereotactic surface projection analysis over visual inspection in discrimination of patients with very early Alzheimer's disease from controls using brain perfusion SPECT. J Nucl Med 2004;45: 1450–7.
16. Sakamoto S, Ishii K. Low cerebral glucose extraction rates in the human medial temporal cortex and cerebellum. J Neurol Sci 2000;172:41–8.
17. Matsuda H. Role of neuroimaging in Alzheimer's disease, with emphasis on brain perfusion SPECT. J Nucl Med 2007; 48:1289–300.

Neuropathology 2008; **28**, 132–142 doi:10.1111/j.1440-1789.2007.00864.x

Original Article

Extensive loss of arterial medial smooth muscle cells and mural extracellular matrix in cerebral autosomal recessive arteriopathy with subcortical infarcts and leukoencephalopathy (CARASIL)

Takashi Oide,[1,5] Hiroshi Nakayama,[2] Sohei Yanagawa,[3] Nobuo Ito,[4] Shu-ichi Ikeda[5] and Kunimasa Arima[1]

[1]Department of Laboratory Medicine, Musashi Hospital, National Center of Neurology and Psychiatry, Kodaira, [2]Department of Neuropsychiatry, Tokyo Metropolitan Neurologic Hospital, Fuchu, Departments of [3]Neurology and [4]Pathology, Iida Municipal Hospital, Iida, and [5]Third Department of Medicine, Shinshu University School of Medicine, Matsumoto, Japan

Cerebral autosomal recessive arteriopathy with subcortical infarcts and leukoencephalopathy (CARASIL) is a distinctive clinicopathologic entity characterized by young adult-onset non-hypertensive vasculopathic encephalopathy accompanied by alopecia and disco-vertebral degeneration. CARASIL arteriopathy is histopathologically characterized by intense arteriosclerosis without the deposition of granular osmiophilic materials. Until now, the obliterative arteriosclerosis is the presumptive cause of subcortical ischemia in CARASIL; however, a detailed vascular pathology leading to diffuse leukoencephalopathy remains unclear. In this study, we examined two autopsied CARASIL brains in comparison with an autopsy case of cerebral autosomal dominant arteriopathy with subcortical infarcts and leukoencephalopathy (CADASIL). Intensity of arterial sclerotic changes of CARASIL was evaluated by sclerotic index analysis. Immunohistochemical investigations were performed using a battery of primary antibodies, which recognized vascular cellular and extracellular components. As a result, sclerotic changes were disclosed to be mild and infrequent in CARASIL, in contrast to CADASIL that showed severe obliterative arterial changes. In CARASIL, conversely, most of the arteries were centrifugally enlarged and some were collapsed. We further revealed that arterial medial smooth muscle cells (SMCs) in patients with CARASIL were extensively lost, even in arteries without sclerotic changes. Arterial adventitia in CARASIL was conspicuously thin and immunoreactivities for type I, III, and VI collagens and fibronectin were appreciably weak in this region, indicating a reduction in the mural extracellular matrix (ECM). Because of the medial and adventitial degeneration, CARASIL brains likely receive marked fluctuations in blood flow because of deviations in the structural and functional basis of autoregulation mechanisms. We thus consider that diffuse leukoencephalopathy in CARASIL may be caused by arterial medial SMC loss with mural ECM reduction. We speculate that the abnormalities in the ECM are causatively related to the SMC degeneration, since the ECM is a crucial signal determining the biophysiological properties of arterial SMCs.

Key words: arteriosclerosis, CADASIL, CARASIL, extracellular matrix, smooth muscle cell.

INTRODUCTION

Cerebral autosomal recessive arteriopathy with subcortical infarcts and leukoencephalopathy (CARASIL), also known as Maeda syndrome, is characterized by young-adult onset vasculopathic subcortical encephalopathy without hypertension and is accompanied by several unique extra-CNS symptoms.[1,2] This clinicopathologic entity was first reported by Maeda *et al.* in three sibling patients from a consanguineous Japanese family in a

Correspondence: Takashi Oide, MD, PhD, Department of Diagnostic Pathology, Graduate School of Medicine, Chiba University, 1-8-1 Inohana, Chuo-ku, Chiba 260-8670, Japan. Email: oide@faculty.chiba-u.jp

Received 23 January 2007; revised 3 September 2007; accepted 4 September 2007.

preliminary form in 1965, and in greater detail in 1976.[3] Following the addition of several similar patients belonging to unrelated families, Fukutake *et al.* proposed the encephalopathy as a new systemic syndrome named "familial young-adult-onset arteriosclerotic leukoencephalopathy with alopecia and lumbago without arterial hypertension".[4,5] To date, more than 20 cases of this syndrome have been reported, exclusively from Japan. Since cerebral autosomal dominant arteriopathy with subcortical infarcts and leukoencephalopathy (CADASIL) has been established as a genetic cerebrovascular disease, Maeda syndrome has begun to attract more attention and is now regarded as a distinctive disease entity and has been re-named "CARASIL", an acronym identifying its autosomal recessive fashion of inheritance.[1,6] Although both CADASIL and CARASIL share the common clinical features of subcortical multi-infarcts and leukoencephalopathy, some notable differences exist between the clinicopathological features of these two disease entities. Clinically, CARASIL and CADASIL are both characterized by severe psychomotor deterioration caused by subcortical encephalopathy, beginning during a patient's twenties to early thirties. In addition to these CNS symptoms, CARASIL features a characteristic constellation of extra-CNS symptoms (alopecia, vertebral disc herniation, and spondylosis deformans) that often precedes the neurologic symptoms. Limb arthropathy and keratotic skin changes are also frequent; however, migraine has never been reported in patients with CARASIL. The prognosis of CARASIL is poorer than that of CADASIL; patients with CARASIL become bedridden within several years of the onset of neurologic symptoms and usually die within 10 years.[5] Nuances in the neuroradiologic findings for CARASIL and CADASIL have also been reported: the leukoencephalopathy in the former is diffuse and homogenous from the incipient stage of the illness, whereas that in the latter is rather punctuated and nodular.[7] Histopathologically, CADASIL is characterized by the degeneration of medial smooth muscle cells (SMCs) accompanied by the deposition of granular osmiophilic materials (GOM) in small arteries and arterioles.[8] On the other hand, CARASIL is characterized by severe arteriosclerosis, but GOM deposition is not seen.[1] Until now, the obliterative arteriosclerosis has been believed to cause leukoencephalopathy in CARASIL; however, a detailed vascular pathology has not been reported, and the precise mechanism leading from the arterial changes to the cerebral white matter degeneration remains unclear. In this report, we histopathologically examined two autopsied CARASIL patients and compared our results with those for CADASIL patients and typical arteriosclerosis cases. We found that the tunica media and adventitia of the arteries were severely affected in CARASIL brains. The significance of medial and adventitial degeneration in the pathogenesis of CARASIL is discussed herein.

METHODS

Patients

Brain tissues from two Japanese patients with CARASIL who were from unrelated consanguineous families were histopathologically studied. Visceral tissues were not available. Their detailed clinical features have been reported elsewhere[1,3] and are summarized in Table 1. Brain MRI findings and gross findings of autopsied brains are also shown in Table 1. Two different populations were selected as controls: four patients with arteriosclerosis and atherosclerosis (3 women and 1 man; mean age, 78.8 ± 11.0 years, range, 68–91 years) as arteriosclerotic controls and seven patients without any particular cerebrovascular pathology (4 with schizophrenia, 1 with polyneuropathy, 1 with dermatomyositis, and 1 with amyotrophic lateral sclerosis; 4 women and 3 men; mean age, 59.8 ± 4.5 years, range, 51–65 years) as nonarteriosclerotic controls. Brain tissue from a 75-year-old Japanese patient with CADASIL who had been fully characterized clinicopathologically was also prepared.[9] The brain tissues were fixed in 10% formalin solution, embedded in paraffin, cut to a thickness of 6 μm, and stained with HE, Klüver-Barrera, Holzer, Bodian, PAS, elastica van Gieson, and elastica Masson stains.

Evaluation of the sclerotic index (SI)

For the sclerotic index (SI) study, two nonarteriosclerotic controls, one arteriosclerotic control having subcortical infarcts, one CADASIL, and two CARASIL were examined. Multiple digital images at the higher magnification were consecutively taken from white matter arteries and leptomeningeal arteries in frontal lobes on HE sections. Those arterial images were numbered serially, and their external and internal diameters were measured by a digital micrometer. Measurements in arteries with elliptical profiles were taken perpendicular to the long axis of the ellipse.[10] Arteries of external caliber ≥50 μm but <200 μm were included in this SI study. SI was defined as "1-(internal diameter/external diameter)".[10] Statistical analysis was carried out using Kuruskal-Wallis test at the significance level of 0.05.

Frequency of cerebral arterial changes

To estimate the frequency of the pathologic findings for the CARASIL cerebrovasculature, one coronal section of the frontal lobe was selected from each CARASIL case and stained using the elastica van Gieson method. The presence or absence of representative pathologic changes was

Table 1 Patient characteristics

Case	Age/sex	Duration (y)	Family history	Blood pressure (mmHg)	Symptoms and signs		Brain MRI	Brain weight (g)	Autopsy gross findings	Ref.
					Neurologic	Extra-CNS				
1	35/M	9	Consanguineous parents. Same disease in siblings	120/60	Rigidity, dementia, dysarthria, pyramidal tract signs	Elbow arthropathy, spondylosis deformans, lumbar intervertebral disc herniation, dry and loose skin, alopecia	Not performed	1310	Diffuse cerebral white matter atrophy, multiple foci of softening in the cerebral white matter, dilated lateral ventricles, marked brainstem atrophy, atheromatous changes in the internal carotid arteries and anterior and middle cerebral arteries	3
2	51/F	17	Consanguineous parents. Same disease in sister	68/50 (after being bedridden)	Pseudobulbar palsy, dementia, hemiparesis, incontinence, pyramidal tract signs	Knee arthropathy	Increased T2 signal intensity diffusely in the cerebral white matter and spotty in the thalamus and pons	850	Moderate cerebral cortical atrophy, marked brainstem atrophy, multiple foci of softening in the cerebral white matter, basal ganglia, and the base of brainstem, moderate atherosclerosis of the large arteries at the base of brain	1